Published in final edited form as:
Invest Radiol. 2011 September ; 46(9): 586–593. doi:10.1097/RLI.0b013e31821c0e84.

Porcine *Ex Vivo* Liver Phantom for Dynamic Contrast-Enhanced Computed Tomography: Development and Initial Results

Scott M. Thompson, B.A.[Medical Scientist Training Program (MSTP)]
College of Medicine, Mayo Clinic, Rochester, MN

Juan C. Ramirez Giraldo, M.S.
Mayo Graduate School, College of Medicine, Mayo Clinic, Rochester, MN

Bruce Knudsen, M.S.[Senior Research Technologist]
Department of Laboratory Medicine and Pathology, College of Medicine, Mayo Clinic, Rochester, MN

Joseph P. Grande, M.D., Ph.D.[Professor of Laboratory Medicine and Pathology]
Department of Laboratory Medicine and Pathology, College of Medicine, Mayo Clinic, Rochester, MN

Jodie A. Christner, Ph.D.
Department of Radiology, College of Medicine, Mayo Clinic, Rochester, MN

Man Xu[Summer Undergraduate Research Student]
College of Medicine, Mayo Clinic, Rochester, MN

David A. Woodrum, M.D., Ph.D.[Assistant Professor of Radiology]
Department of Radiology, College of Medicine, Mayo Clinic, Rochester, MN

Cynthia H. McCollough, Ph.D.[Professor of Radiologic Physics]
Department of Radiology, College of Medicine, Mayo Clinic, Rochester, MN

Matthew R. Callstrom, M.D., Ph.D.[Assistant Professor of Radiology]
Department of Radiology, Mayo Clinic, Rochester, MN

Abstract

Objectives—To demonstrate the feasibility of developing a fixed, dual-input, biological liver phantom for dynamic contrast-enhanced computed tomography (CT) imaging and to report initial results of use of the phantom for quantitative CT perfusion imaging.

Materials and Methods—Porcine livers were obtained from completed surgical studies and perfused with saline and fixative. The phantom was placed in a body-shaped, CT-compatible acrylic container and connected to a perfusion circuit fitted with a contrast injection port. Flow-controlled contrast-enhanced imaging experiments were performed using a 128-slice and 64 slice, dual-source multidetector CT scanners. CT angiography protocols were employed to obtain portal venous and hepatic arterial vascular enhancement, reproduced over a period of four to six months. CT perfusion protocols were employed at different input flow rates to correlate input flow with

Corresponding Author Scott M. Thompson, B.A., Medical Scientist Training Program (MSTP), Mayo Clinic, 200 First Street Southwest, Rochester, MN 55905, USA, Fax: (507) 266-1657, Phone: (507) 250-3902, thompson.scott@mayo.edu.

calculated tissue perfusion, to test reproducibility and demonstrate the feasibility of simultaneous dual input liver perfusion. Histologic analysis of the liver phantom was also performed.

Results—CT angiogram 3D reconstructions demonstrated homogenous tertiary and quaternary branching of the portal venous system out to the periphery of all lobes of the liver as well as enhancement of the hepatic arterial system to all lobes of the liver and gallbladder throughout the study period. For perfusion CT, the correlation between the calculated mean tissue perfusion in a volume of interest and input pump flow rate was excellent ($R^2 = 0.996$) and color blood flow maps demonstrated variations in regional perfusion in a narrow range. Repeat perfusion CT experiments demonstrated reproducible time-attenuation curves and dual-input perfusion CT experiments demonstrated that simultaneous dual input liver perfusion is feasible. Histologic analysis demonstrated that the hepatic microvasculature and architecture appeared intact and well preserved at the completion of four to six months of laboratory experiments and contrast enhanced imaging.

Conclusions—We have demonstrated successful development of a porcine liver phantom using a flow-controlled extracorporeal perfusion circuit. This phantom exhibited reproducible dynamic contrast-enhanced CT of the hepatic arterial and portal venous system over a four to six month period.

Keywords

Perfusion Imaging; Computed Tomography; Biological Phantom; Porcine

INTRODUCTION

Dynamic contrast-enhanced Perfusion Computed Tomography (CT) has emerged as a powerful tool for the functional evaluation of tissue perfusion in a variety of clinical and research applications, particularly in the assessment of vascular and oncologic diseases.[1–3] Perfusion CT techniques measure the temporal changes in tissue enhancement after injection of contrast medium.[4] Perfusion imaging has been studied and validated clinically most extensively in the evaluation of cerebral blood flow in acute ischemic stroke owing to the lack of motion within the brain[5, 6] In recent years, perfusion CT has found further applications outside of the brain in numerous tissues for the diagnosis, grading, staging, prognostic evaluation and therapeutic planning and monitoring of various diseases.[3, 7, 8]

Although perfusion CT has been studied for nearly 3 decades, several technological and practical limitations have restricted its clinical use, such as: limited scan range, temporal resolution and radiation dose.[3] Furthermore, specific applications such as body perfusion are also hampered by respiratory motion artifacts and organ deformability.[3, 9] However, recent advances in multidetector CT systems seem to address some of the aforementioned limitations, due to the current availability of scanners with faster rotation times and larger scanning ranges. The larger anatomic coverage can be accomplished by using wider detector coverage,[10] axial scanning at two interleaved table positions (`toggling' table),[11, 12] or dynamic spiral scanning, where the table moves fluidly back and forth through the gantry.[13, 14] Additional advances include, improved sensitivity of x-ray detectors, and improvements in image quality (spatial resolution and low contrast detectability).[15]

In spite of tremendous progress in perfusion CT, several challenges still persist. First, radiation dose must be considered.[16] Although current clinical perfusion CT exams, such as brain perfusion CT, are considered safe when properly performed, there is a need for reducing radiation dose to the lowest possible level without sacrificing the validity of the clinical information.[17] Furthermore, concerns have been raised about variations in the accuracy of the technique due to different scanners, scanning techniques, contrast medium

protocols, perfusion models, and post-processing algorithms.[18–23] Although perfusion CT aims to be a quantitative tool for measuring tissue perfusion, there is little standardization in the techniques used and the quantitative results need further validation, particularly with respect to their role in clinical decision-making outside the brain.

As a result of the aforementioned limitations, there exists a critical need to examine the perfusion CT technique in a controlled, systematic manner. However, because this technique requires ionizing radiation and iodinated intravenous contrast material, it is not practical or ethical to study body perfusion CT in patients repeatedly over time. Although studying perfusion in *in vivo* animal models is possible, there are several challenges to consider, including the trade-offs between small and large animal models, physiological changes caused by the use of contrast agents, drugs, or anesthesia (which affect the repeatability of the experiments) and the cost of repeated scanning and animal maintenance. Experimental phantom models using tubing arrays of varying geometries exist, but do not necessarily represent the complexity of the human vasculature and microcirculation,[24] although several of these engineered phantoms have been proposed for US, CT and MR imaging.[25–30] Alternatively, the use of fresh animal organ phantoms that mimic human vasculature very well have been proposed, but suffer from a narrow experimental time window.[31, 32] More recently, Haberland et al., reported on the development of a fixed porcine kidney phantom for studying renal perfusion with CT that allows for reproducible measurements in a controlled environment over time.[33] These studies suggest a promising methodology for studying scan protocols and post-processing algorithms with fixed *ex vivo* biological phantoms.

We report here the development of a fixed, dual-input, *ex vivo* liver phantom for dynamic contrast-enhanced CT imaging and initial results of use of the phantom for quantitative CT perfusion imaging.

MATERIALS AND METHODS

Phantom Creation

Porcine livers (N=5) were obtained immediately following completion of IACUC-approved surgical research studies from 55–65 kilogram adult, domestic female pigs. Each pig was given 5000U IV heparin prior to euthanasia. The common bile duct and principle hepatic vasculature, including the portal vein (PV), common hepatic artery (HA) and infra- and suprahepatic vena cava (iIVC and sIVC), were identified, ligated and cut and the liver was mobilized. Following explantation, the HA, PV and sIVC were each cannulated with Tygon tubing (3–4mm, 9–10mm and 12–13mm respectively) of appropriate diameter and secured with circumferential 2-0 silk suture. The liver was transferred to the laboratory within one hour of euthanasia and placed in a 0.9% normal saline bath, visceral surface facing up for drainage out of the sIVC. The PV and HA were connected to a primed, Masterflex® L/S™ peristaltic pump (Cole-Parmer Instrument Co., Bunker, CT) and perfused with warmed (37°C), heparanized saline (100,000 units in 18.9L 0.9% NaCl) for approximately one hour until the venous effluent drained clear. This was followed by a solution of 10% neutral buffered formalin (Fisher Scientific/Acros, Waltham, MA) perfused through the PV and HA for ten to fifteen minutes (Figure 1A). The HA, PV and sIVC were clamped off in a filled state and the liver was submerged in the formalin solution to complete fixation by diffusion. The liver was stored in a sealed container at 21°C and allowed to fix for a minimum of five days. Of the five livers harvested, the initial two were used to optimize the surgical, perfusion and fixation procedures. Based on the optimization of the experimental setup in the laboratory, the next three livers were used for the imaging experiments.

Laboratory phantom perfusion experiments

Following fixation, the liver was removed from the fixative solution and submerged in a 0.9% saline bath. Using the same method described above, 0.9% saline was perfused through the PV and HA separately to rinse out the formalin from the vasculature and confirm vessel patency. Next, to determine the input flow range (ml/min) through the liver, the portal vein was connected to a Bio-Medicus® 560 (Medtronic Inc., Minneapolis, MN) perfusion circuit with flow (ml/min) and pressure (mmHg) transducers incorporated into the circuit and the hepatic artery was connected to the peristaltic pump described above. The PV was selectively perfused with 0.9% saline at different input flow rates by adjusting the manual knob on the pump controller, thereby increasing the revolutions per minute (RPMs) of the external pump drive motor and subsequently, the flow rate in the perfusion circuit. After a period of flow equilibration, the flow and pressure in the circuit were recorded from the console. The hepatic artery was selectively perfused with 0.9% saline at different input flow rates by adjusting the manual knob on the pump controller, thereby increasing the speed of the pump roller. The flow through the hepatic artery at each pump level was estimated by collecting the output perfusate over 120 seconds and dividing the volume by the time. Following each experiment, the phantom was flushed with 0.9% saline, reperfused with fixative and stored as previously described. The purpose of this procedure was to maintain the patency of the hepatic vasculature and microcirculation over time.

Dynamic Contrast-Enhanced Computed Tomography (CT) Imaging

Prior to scanning, each liver was removed from the fixative solution and the perfusion technique described above was reestablished. The liver was placed in a body-shaped, CT compatible acrylic container—30 cm in lateral dimension and 27 cm in anterior-posterior dimension—and set on a raised platform to allow the suprahepatic IVC to drain unobstructed outside of the container via Tygon tubing. The phantom container was then filled with 0.9% saline to completely submerge the liver. For vascular imaging, the PV and HA were perfused separately with 0.9% saline and flushed until a steady stream drained from the IVC. For single input perfusion imaging, the PV was connected to the perfusion pump (Bio-Medicus® 560) for the flow controlled perfusion experiments (250, 375, 500, 625 and 750 ml/min) (Table 1). For simultaneous dual input perfusion imaging, the PV was connected to the Bio-Medicus® 560 perfusion pump and the HA to the Masterflex® L/S™ peristaltic pump to simulate the continuous and pulsatile flow through each respective vessel and allow for a flow controlled perfusion experiment (PV: 250 ml/min and HA: 80 ml/min). Contrast-injection ports were incorporated into the perfusion circuits to allow access for controlled contrast injection (Figure 1B).

Scanning protocols

Single input imaging—The liver phantom was scanned using a 128-slice, dual-source, multidetector CT scanner (Definition Flash, Siemens Healthcare, Forcheim, Germany). A perfusion CT protocol (Protocol A) was employed to correlate input flow within the system to the liver perfusion calculated by the manufacturer software. This protocol was performed at five input flow rates. CT scanning parameters included: 100 kVp, 150 mAs, 32 × 1.2 mm collimation, 38.4 mm scan range, zero table feed, 500 ms rotation time and 45 s total scan time. This resulted in 90 total volumetric datasets. The radiation output of the scanner, as reflected by the console CTDIvol was 566.36 mGy. A second perfusion CT protocol (Protocol B) was employed consisting of a sequence of two perfusion scans under identical scanning and setup conditions, to evaluate the reproducibility of the time attenuation curves. Scanning parameters were identical to Protocol A except that scanning time was longer (59.4 s) in order to capture the dynamics of the time-attenuation curve from start to contrast washout. Cycle time was 1s, for a total of 60 volumetric datasets. The console CTDIvol was

375.01 mGy. Protocol B was repeated after thirty minutes following two intervening contrast-enhanced scans. Images from both protocols A and B were reconstructed using a medium smooth kernel (B25) and 5 mm slice thickness.

The entire length of the phantom was also scanned with a CT angiography (CTA) protocol, performed using 120 kVp, 125 effective mAs, 64 × 0.6 mm collimation, 500 ms rotation time, and pitch = 0.6. The console CTDIvol was 8.43 mGy for each acquisition. CTA images were reconstructed using a medium-sharp kernel (B40), 0.75 mm slice thickness, and volume rendered using manufacturer software (Syngo, Siemens Healthcare). The CTA protocol was performed to obtain portal venous and hepatic arterial maps right after phantom creation, as well as at 4 to 6 months, prior to histological analysis of the liver specimen.

Dual input imaging—To demonstrate the feasibility of simultaneous dual input liver perfusion imaging, the liver phantom was scanned using a 64-slice, dual-source, multidetector CT scanner (Definition, Siemens Healthcare, Forcheim, Germany). A perfusion CT protocol (Protocol C) was performed at a single flow rate for both the PV (250ml/min) and HA (80 ml/min). CT scanning parameters included: 80 kVp, 150 mAs, 24 × 1.2 mm collimation, 28.8 mm scan range, zero table feed, 1000 ms rotation and 1.5 cycle time, for a total scan time of 52.5 s. Console CTDIvol was 89.75 mGy. Images were reconstructed using medium smooth kernel (B20) and 1.5 mm slice thickness.

Contrast injection protocols

Single Input—All experiments employed a non-ionic-iodinated contrast agent (Omnipaque 300, GE Healthcare) and used an automated power injector (Stellant D CT, Medrad Inc, Indianola, PA). For the CTA scans, 5 mL of contrast at an iodine concentration of 300 mg/ml was injected at 5 mL/s. Protocol A was used for a total of five PCT scans, at different flow rates. A constant injection time of approximately three seconds was maintained with the purpose of maintaining a sharp bolus (Table 1). Injection and scanning was started simultaneously, allowing typically 3 to 6 baseline unenhanced scans prior to the arrival of contrast media. Protocol B was performed twice with perfusate at 500 ml/min, contrast injection rate of 2.5 mL/s and a volume of 5 mL of contrast agent. To allow for contrast agent clearance from the liver, saline was perfused for five to ten minutes between scanning.

Dual Input—Perfusion CT Protocol C used consecutive manual injections of 4 ml of contrast agent into both the hepatic arterial and portal venous perfusion circuits separated by 10 seconds and scanning was initiated 6 seconds thereafter. Although only 4 specific scanning protocols are reported here, each liver was imaged over sixty times over the course of four to six months as the perfusion circuit underwent numerous modifications to optimize the experimental setup and image timing.

Data Analysis

Data were evaluated with commercially available 3D perfusion software (syngo Volume Perfusion CT Body, Siemens, Forchheim). A region of interest (ROI) was defined over several central sections of the liver parenchyma on the maximal intensity projection (MIP) images to create a volume of interest (VOI). The vascular input function was taken from the portal vein and/or hepatic artery entering the liver at a position perpendicular to the z-axis. Tissue perfusion parameters were calculated using a maximum-slope method.[34] The mean tissue perfusion (ml/min/100ml) in the VOI was correlated with the input pump flow (ml/min) using the Pearson correlation coefficient. Comparison of time-attenuation curves (TACs), under identical scanning and perfusion conditions, was performed using custom

made software to calculate not only the TACs but also the normalized mean squared error (NMSE), using Matlab version 2009a (Mathworks, Natick, MA). For the simultaneous dual input perfusion experiment, regions of interest (ROIs) were segmented onto a MIP image (Figure 6A) over branches of the hepatic artery and portal vein and liver tissue and TACs were calculated using Matlab 2009a.

4. Histology

Following completion of four to six months of laboratory experiments and 60 contrast-enhanced imaging studies, representative tissue samples were taken from the liver to evaluate the hepatic architecture and patency of the microvasculature. Several 1-cm samples were carefully excised from the periphery of segment II of the left lateral lobe. The specimens were placed in 10% neutral buffered formalin (Fisher Scientific/Acros, Waltham, MA), embedded in paraffin, sectioned with a microtome and stained with hematoxylin-eosin (H&E) to outline the hepatic architecture. The slides were evaluated by light microscopy by an experienced pathologist (20 years).

RESULTS

1. Laboratory Phantom Perfusion Experiments

Following initial preparation and fixation, perfusion of the liver phantom via the PV and HA resulted in steady drainage out of the suprahepatic IVC with negligible leakage from the liver parenchyma. This suggested movement of the perfusate from the intravascular space into the portal tracts and out the hepatic venous system providing initial evidence for the patency of the hepatic microvasculature. Quantitative evaluation of the portal venous flow through the liver at different revolutions per minutes (RPMs) was conducted at a flow range of 200 ml/min to 1300 ml/min. Flow increased linearly ($R^2 = 0.99$) as the pressure in the circuit increased from 12 mmHg to 123 mmHg (Table 2). There was no evidence of compromise of the liver capsule at a flow of 1300 ml/min but due to the fixed vascular resistance, flow was not increased further in order to prevent any injury to the hepatic microcirculation. Flow in the hepatic artery was estimated at a flow range of 80ml/min to 150ml/min, demonstrating significantly lower flow and smaller dynamic range compared to the portal venous flow. The peristaltic pump speed was not increased further due to high pressure on palpation of the hepatic arterial input relative to the portal venous input.

2. Dynamic Contrast Enhanced Imaging CT Imaging

Dynamic contrast-enhanced CT imaging was successfully performed on the liver phantoms over the course of four to six months. Of the three livers prepared for imaging experiments, all were used for vascular imaging whereas two were selected for perfusion imaging. The portal venous CTA and hepatic arterial system CTA were performed separately to evaluate the vascular enhancement of the phantom. 3D reconstruction demonstrated homogenous tertiary and quaternary branching of the portal venous system out to the periphery of all lobes of the liver (Figure 2A & B). The gallbladder did not demonstrate enhancement with injection of the portal vein, as expected. MIP images demonstrated enhancement of the hepatic arterial system to all lobes of the liver as well as the cystic artery to the gallbladder (Figure 2C).

In the phantom selected for single input quantitative perfusion imaging and reproducibility experiments, the correlation between the calculated mean tissue perfusion in a VOI and input pump flow rate was excellent ($R^2 = 0.996$) (Figure 3). MIP image (Figure 4A) and corresponding color blood flow (ml/min/100ml) map (Figure 4B) demonstrated variations in regional perfusion across a narrow range. We repeated two identical perfusion scans at an input pump flow rate of 500 ml/min separated by two contrast-enhanced scans and 15 L of

perfusate to compare the time-attenuation curves (TAC). 500 ml/min was selected for the flow rate because it was middle of the range used for the perfusion experiments but any flow rate in the dynamic range (200 ml/min to 1300 ml/min) could have been chosen to evaluate reproducibility of the TACs. The TACs of the vessel input functions demonstrated a 6.7 % normalized mean squared error (NMSE) difference while the liver tissue perfusion in a selected ROI demonstrated a NMSE difference of approximately 0.43 % (Figure 5). The TACs also show a monophasic injection protocol, and reveal the bolus as compact and symmetric with a steep ascent and descent. In the phantom selected for dual input perfusion imaging, TACs revealed biphasic liver enhancement with the hepatic arterial peak enhancement preceding the portal venous peak enhancement (Figure 6B).

3. Histology

Representative H&E stained sections from the periphery of segment II demonstrated remarkable preservation of the hepatic architecture, with patent portal tracts (Figure 7A). The portal vein and hepatic artery were also patent, with preservation of endothelial cells (Figure 7B). There was no evidence of hepatocyte necrosis.

DISCUSSION

In this study, we report on the development of a fixed, dual-input biological liver phantom using an *ex vivo* porcine liver and the results from initial pilot and feasibility experiments using this phantom for dynamic contrast-enhanced CT imaging studies. To the best of our knowledge, this is the first fixed biological liver phantom designed for dynamic contrast-enhanced CT imaging studies.

Using the techniques described in this paper for the surgical procedure and subsequent perfusion and fixation, we successfully connected the liver phantom to a flow-controlled extracorporeal perfusion circuit and imaged it with both single and dynamic contrast-enhanced CT repeatedly over an extended time with excellent stability and retention of patency. We found homogenous enhancement of the portal venous system to the periphery of all lobes of the liver phantom (Figures 2A –2B). The hepatic arterial system also enhanced with perfusion of all lobes of the liver and the gallbladder (Figure 2C). The vascular imaging results were consistent with the histologic analysis of the liver phantom tissue at the end of the study period which demonstrated excellent maintenance of the hepatic architecture and patency of the microcirculation (Figures 7A–7B). The vascular imaging and histologic results taken together support the use of perfusion fixation to prepare the phantom. This approach resulted in vascular enhancement throughout the phantom, suggesting our methodology allowed for preservation of the maximum liver volume while preserving the hepatic vasculature and microcirculation.

Post fixation, the liver phantom allowed perfusion at a wide-range of physiologically relevant input flows for hepatic circulation (80ml/min to 1300 ml/min).[35, 36] These results are similar to data reported for *in vivo* and *ex vivo* non-fixed porcine liver vascular flow rates.[37] However, fixation may reduce the upper flow limit due to loss of vascular distensibility, particularly in the hepatic arterial system, and alter the physiological perfusion pressures (Table 2). We found excellent correlation between mean tissue perfusion in the liver as a function of the input perfusate flow rate (Figure 3). These results are comparable to those for a kidney phantom reported by Haberland et al.[33] The color perfusion flow maps of the phantom demonstrated widespread tissue perfusion with regional variation in a narrow range, as would be expected (Figure 4). Analysis of numerous images from different flow-controlled liver perfusion scans did not reveal any areas of non-perfusion. Likewise, when the liver phantom was imaged under identical scan protocols and experimental parameters at different time points, this resulted in remarkably similar time-attenuation

curves for the vascular input functions and tissue ROIs, demonstrating the stability of the phantom (Figure 5).

The simultaneous dual input perfusion imaging experiment demonstrated enhancement of both the arterial and venous inputs, as well as a biphasic time-attenuation-curve (TAC) within the liver tissue (Figure 6B). Since only manual injections were available at the time of this experiment, a time delay built-in before the scanning sequence, to avoid operator exposure, resulted in limited recording of the ascent of the arterial TAC.

Our study had several acknowledged limitations. First, although the experiments reported here demonstrate the feasibility of both separate and simultaneous dual input liver imaging within physiological flow rates for the hepatic circulation, it must be noted that the simultaneous dual input perfusion experiments did not accurately recreate physiological liver perfusion, which will require careful control of variables such as contrast injection timing, injection rates, and contrast volumes and concentrations. Accurate biphasic liver perfusion imaging simulation with the phantom then will be the subject of future work. Notice however, that the remarkable reproducibility of the TACs using only one input (e.g. portal vein), provides an excellent tool for protocol optimization. Another limitation was that the pressure was measured directly from the perfusion circuit, which might not reflect the actual pressure at the vessel inputs. In addition, the pressure in the hepatic arterial perfusion circuit was not measured due to use of a peristaltic pump and incompatibility with the pressure transducer. An ideal physiological liver model would recapitulate the higher pressure in the hepatic arterial system and lower pressure in the portal venous system. However, fixation of the liver results in loss of vascular compliance and the resulting pressures within the vascular system may no longer reflect the true physiologic parameters. Subjective in evaluation, palpation of the hepatic arterial input did reveal a noticeably higher pressure compared to the portal venous input vessel, at even a low flow rate. A final limitation was that these perfusion studies were performed on fixed *ex vivo* tissue with a saline perfusate. Understanding the significance of this limitation will require correlation with porcine liver perfusion time-attenuation curves *in vivo*. The performed experiments elucidated several considerations for further refinement of the experimental setup for simultaneous dual input liver perfusion and is the subject of future work. Finally, it must be noted that both an understanding of the porcine hepatic vascular anatomy[38] and careful initial surgical dissection and perfusion-fixation of the liver are critical to the success of the phantom for later experimentation.

There are several potential applications for using the liver phantom for systematic perfusion imaging studies. Most importantly, the phantom will be helpful for determining the effects of radiation dose reduction on perfusion quantification accuracy, testing the effect of noise reduction algorithms, contrast injection protocols and different scanning acquisition strategies.[39, 40] Beyond diagnostic imaging studies, *ex vivo* perfused animal organ phantoms would be useful for studying biothermal properties such as tissue perfusion that impact interventional thermal ablation techniques, including high intensity focused ultrasound (HIFU) and radiofrequency ablation.[41–43]

Conclusion

In this study we have demonstrated the development of an *ex vivo* perfused liver phantom for dynamic contrast-enhanced CT imaging. We also demonstrated that this liver phantom can provide a highly reproducible and realistic model for physiological perfusion imaging of the liver or other organs (when using only one input). This liver phantom has the potential to serve as a model for studying both diagnostic and interventional imaging applications. Future work will aim to recapitulate *in vivo* liver perfusion in the *ex vivo* model as closely as possible through further refinement of the experimental setup.

Acknowledgments

Infrastructure support provided by NIH construction grant NIH C06 RR018898 and Center for Translational Science Activities (CTSA) grant NIH UL1 RR024150.

Support provided by NIH construction grant NIH C06 RR018898 and Center for Translational Science Activities (CTSA) grant NIH UL1 RR024150. The authors thank Dr. Lilach O. Lerman M.D., Ph.D., James D. Krier, John R. Woollard, and John A. Crane for providing access to porcine livers and Jeffrey B. Riley, C.C.P. for providing equipment and advice on the perfusion setup.

REFERENCES

1. Miles KA. Functional computed tomography in oncology. Eur J Cancer. 2002; 38:2079–2084. [PubMed: 12387833]
2. Wintermark M, Sincic R, Sridhar D, et al. Cerebral perfusion CT: technique and clinical applications. J Neuroradiol. 2008; 35:253–260. [PubMed: 18466974]
3. Kambadakone AR, Sahani DV. Body perfusion CT: technique, clinical applications, and advances. Radiol Clin North Am. 2009; 47:161–178. [PubMed: 19195541]
4. Miles KA. Measurement of tissue perfusion by dynamic computed tomography. Br J Radiol. 1991; 64:409–412. [PubMed: 2036562]
5. Axel L. Cerebral blood flow determination by rapid-sequence computed tomography: theoretical analysis. Radiology. 1980; 137:679–686. [PubMed: 7003648]
6. Hoeffner EG, Case I, Jain R, et al. Cerebral perfusion CT: technique and clinical applications. Radiology. 2004; 231:632–644. [PubMed: 15118110]
7. Goetti R, Leschka S, Desbiolles L, et al. Quantitative computed tomography liver perfusion imaging using dynamic spiral scanning with variable pitch: feasibility and initial results in patients with cancer metastases. Invest Radiol. 2010; 45:419–426. [PubMed: 20498611]
8. Choi SH, Chung JW, Kim HC, et al. The role of perfusion CT as a follow-up modality after transcatheter arterial chemoembolization: an experimental study in a rabbit model. Invest Radiol. 2010; 45:427–436. [PubMed: 20440211]
9. Nakashige A, Horiguchi J, Tamura A, et al. Quantitative measurement of hepatic portal perfusion by multidetector row CT with compensation for respiratory misregistration. Br J Radiol. 2004; 77:728–734. [PubMed: 15447957]
10. Siebert E, Bohner G, Dewey M, et al. 320-slice CT neuroimaging: initial clinical experience and image quality evaluation. Br J Radiol. 2009; 82:561–570. [PubMed: 19221186]
11. Furtado AD, Lau BC, Vittinghoff E, et al. Optimal brain perfusion CT coverage in patients with acute middle cerebral artery stroke. AJNR Am J Neuroradiol. 2010; 31:691–695. [PubMed: 19942712]
12. Roberts HC, Roberts TP, Smith WS, et al. Multisection dynamic CT perfusion for acute cerebral ischemia: the “toggling-table” technique. AJNR Am J Neuroradiol. 2001; 22:1077–1080. [PubMed: 11415901]
13. Haberland U, Klotz E, Abolmaali N. Performance assessment of dynamic spiral scan modes with variable pitch for quantitative perfusion computed tomography. Invest Radiol. 2010; 45:378–386. [PubMed: 20440213]
14. Christner JA, Stierstorfer K, Primak AN, et al. Evaluation of z-axis resolution and image noise for nonconstant velocity spiral CT data reconstructed using a weighted 3D filtered backprojection (WFBP) reconstruction algorithm. Med Phys. 2010; 37:897–906. [PubMed: 20229899]
15. Yu L, Liu X, Leng S, et al. Radiation dose reduction in CT: Techniques and future perspective. Imaging in Medicine. 2009; 1:65–84.
16. Wintermark M, Lev MH. FDA investigates the safety of brain perfusion CT. AJNR Am J Neuroradiol. 2010; 31:2–3. [PubMed: 19892810]
17. Liu X, Primak AN, Krier JD, et al. Renal perfusion and hemodynamics: accurate in vivo determination at CT with a 10-fold decrease in radiation dose and HYPR noise reduction. Radiology. 2009; 253:98–105. [PubMed: 19789255]

18. Kudo K, Sasaki M, Yamada K, et al. Differences in CT perfusion maps generated by different commercial software: quantitative analysis by using identical source data of acute stroke patients. Radiology. 2010; 254:200–209. [PubMed: 20032153]
19. Bae KT. Intravenous contrast medium administration and scan timing at CT: considerations and approaches. Radiology. 2010; 256:32–61. [PubMed: 20574084]
20. Heiland S, Erb G, Ziegler S, et al. Where contrast agent concentration really matters - a comparison of CT and MRI. Invest Radiol. 2010; 45:529–537. [PubMed: 20661143]
21. Goh V, Halligan S, Hugill JA, et al. Quantitative assessment of colorectal cancer perfusion using MDCT: inter- and intraobserver agreement. AJR Am J Roentgenol. 2005; 185:225–231. [PubMed: 15972428]
22. Goh V, Halligan S, Hugill JA, et al. Quantitative colorectal cancer perfusion measurement using dynamic contrast-enhanced multidetector-row computed tomography: effect of acquisition time and implications for protocols. J Comput Assist Tomogr. 2005; 29:59–63. [PubMed: 15665684]
23. Goh V, Liaw J, Bartram CI, et al. Effect of temporal interval between scan acquisitions on quantitative vascular parameters in colorectal cancer: implications for helical volumetric perfusion CT techniques. AJR Am J Roentgenol. 2008; 191:W288–292. [PubMed: 19020217]
24. Rappaport AM. Hepatic blood flow: morphologic aspects and physiologic regulation. Int Rev Physiol. 1980; 21:1–63. [PubMed: 6993392]
25. Kegeles LS, Stritzke P, Kupfer S, et al. Organ perfusion by dynamic scintigraphy convection-diffusion tracer kinetics in a phantom. Am J Physiol. 1992; 263:F963–973. [PubMed: 1443185]
26. Hindle AJ, Perkins AC. A perfusion phantom for the evaluation of ultrasound contrast agents. Ultrasound Med Biol. 1994; 20:309–314. [PubMed: 8059492]
27. Noguchi T, Yoshiura T, Hiwatashi A, et al. Quantitative perfusion imaging with pulsed arterial spin labeling: a phantom study. Magn Reson Med Sci. 2007; 6:91–97. [PubMed: 17690539]
28. Teslow TN, Robb RA. X-ray computed tomographic (CT) phantom designed for the development of techniques for measurement of myocardial perfusion. Phys Med Biol. 1991; 36:1407–1413. [PubMed: 1745664]
29. Ebrahimi B, Swanson S, Chupp T. A Microfabricated Phantom for Quantitative MR Perfusion Measurements: Validation of Singular Value Decomposition Deconvolution Method. IEEE Trans Biomed Eng. 2010
30. Maciak A, Kronfeld A, Muller-Forell W, et al. A Capillary-Based Perfusion Phantom for the Simulation of Brain Perfusion for MRI. Rofo. 2010
31. Biederer J, Heller M. Artificial thorax for MR imaging studies in porcine heart-lung preparations. Radiology. 2003; 226:250–255. [PubMed: 12511698]
32. Risse F, Boese JM, Hess T, et al. An experimental organ model for magnetic resonance imaging. Z Med Phys. 2007; 17:205–211. [PubMed: 17879818]
33. Haberland U, Cordes J, Lell M, et al. A biological phantom for contrast-media-based perfusion studies with CT. Invest Radiol. 2009; 44:676–682. [PubMed: 19724231]
34. Klotz E, Konig M. Perfusion measurements of the brain: using dynamic CT for the quantitative assessment of cerebral ischemia in acute stroke. Eur J Radiol. 1999; 30:170–184. [PubMed: 10452715]
35. Eipel C, Abshagen K, Vollmar B. Regulation of hepatic blood flow: the hepatic arterial buffer response revisited. World J Gastroenterol. 2010; 16:6046–6057. [PubMed: 21182219]
36. Richardson PD. Physiological regulation of the hepatic circulation. Fed Proc. 1982; 41:2111–2116. [PubMed: 6804268]
37. Muller SA, Pianka F, Schobinger M, et al. Computer-Based Liver Volumetry in the Liver Perfusion Simulator. J Surg Res. 2010
38. Gravante G, Ong SL, Metcalfe M, et al. The Porcine Hepatic Arterial Supply, Its Variations and Their Influence on the Extracorporeal Perfusion of the Liver. J Surg Res. 2009
39. Brix G, Lechel U, Petersheim M, et al. Dynamic contrast-enhanced CT studies: balancing patient exposure and image noise. Invest Radiol. 2011; 46:64–70. [PubMed: 20881865]

40. Behrendt FF, Jost G, Pietsch H, et al. Computed tomography angiography: the effect of different chaser flow rates, volumes, and fluids on contrast enhancement. Invest Radiol. 2011; 46:271–276. [PubMed: 21368589]

41. Arefiev A, Prat F, Chapelon JY, et al. Ultrasound-induced tissue ablation: studies on isolated, perfused porcine liver. Ultrasound Med Biol. 1998; 24:1033–1043. [PubMed: 9809637]

42. Hildebrand P, Kleemann M, Roblick U, et al. Development of a perfused ex vivo tumor-mimic model for the training of laparoscopic radiofrequency ablation. Surg Endosc. 2007; 21:1745–1749. [PubMed: 17332954]

43. Dragonu I, de Oliveira PL, Laurent C, et al. Non-invasive determination of tissue thermal parameters from high intensity focused ultrasound treatment monitored by volumetric MRI thermometry. NMR Biomed. 2009; 22:843–851. [PubMed: 19562728]

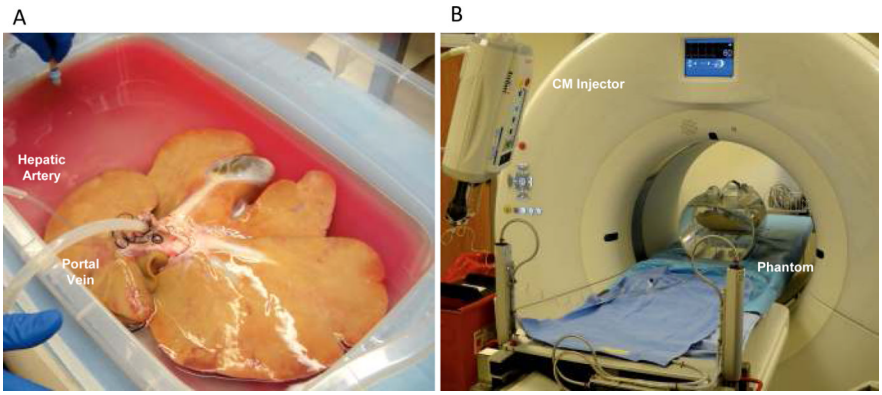

Figure 1. Phantom Creation and Imaging Setup

(A) Initial perfusion and fixation of porcine liver with a heparanized saline solution followed by 10% neutral buffered formalin. **(B)** Perfusion setup for single and dynamic contrast enhanced computed tomography (DCE-CT) in 128-slice, dual-source, multidetector CT scanner (Definition Flash; Siemens Healthcare, Forcheim, Germany). Phantom connected to the perfusion circuit and power injector for contrast imaging.

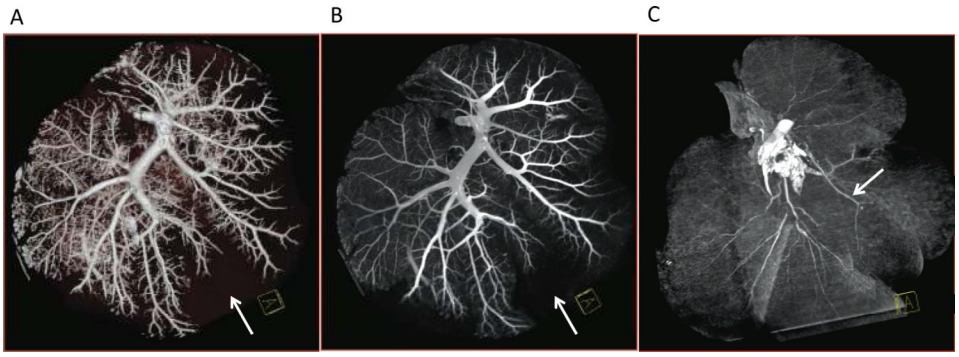

Figure 2. Maximum intensity projection (MIP) images of hepatic vasculature from CT angiogram (CTA) protocol

(A) MIP image 3D reconstruction demonstrating tertiary and quaternary branching of the portal venous system to the periphery of the liver. Note the area absent of vasculature where the gallbladder resides (arrow). **(B)** Portal venous enhancement. **(C)** Hepatic arterial enhancement. Note the cystic artery approaching the gallbladder fossa (arrow).

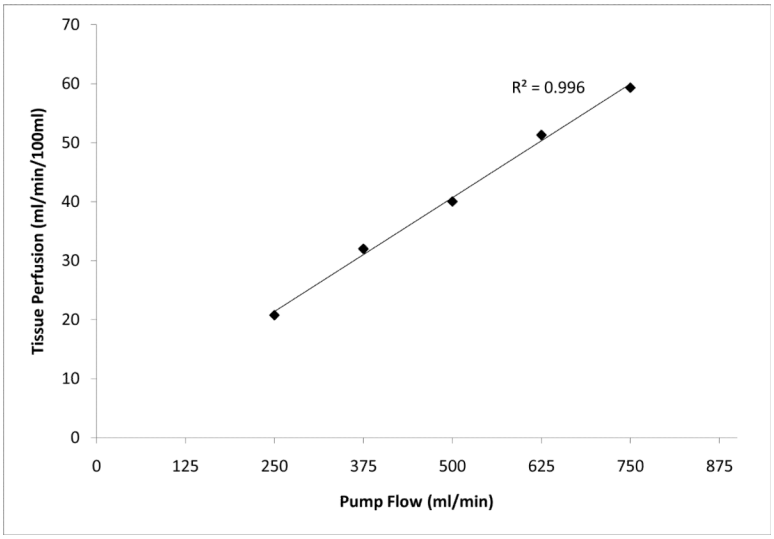

Figure 3. Tissue perfusion vs. input flow

Measured mean tissue perfusion (ml/min/100g) as a function of input flow (ml/min) for a segmented volume of liver.

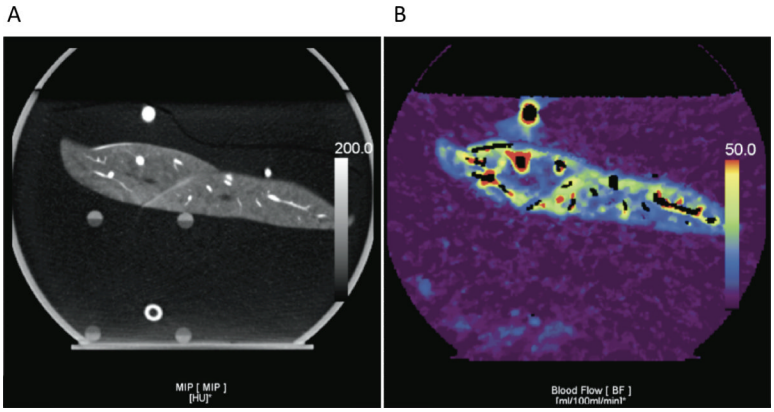

Figure 4. Color Perfusion Map

(A) Volume of Interest (VOI) segmented onto MIP images over a central slice of the liver. **(B)** Corresponding color map of blood flow (ml/min/100ml), demonstrating variation in regional perfusion over a narrow range.

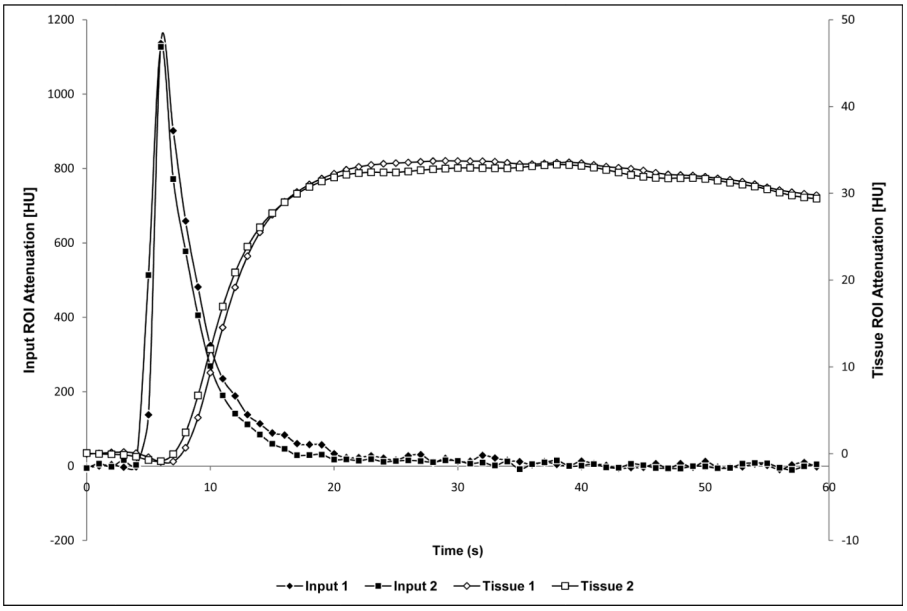

Figure 5. Reproducibility experiments

Time-attenuation curves at the same flow rate demonstrating reproducibility of the technique: Vessel Input ROI with normalized mean squared error (NMSE) = 6.7% and Liver Tissue ROI with NMSE = 0.43%

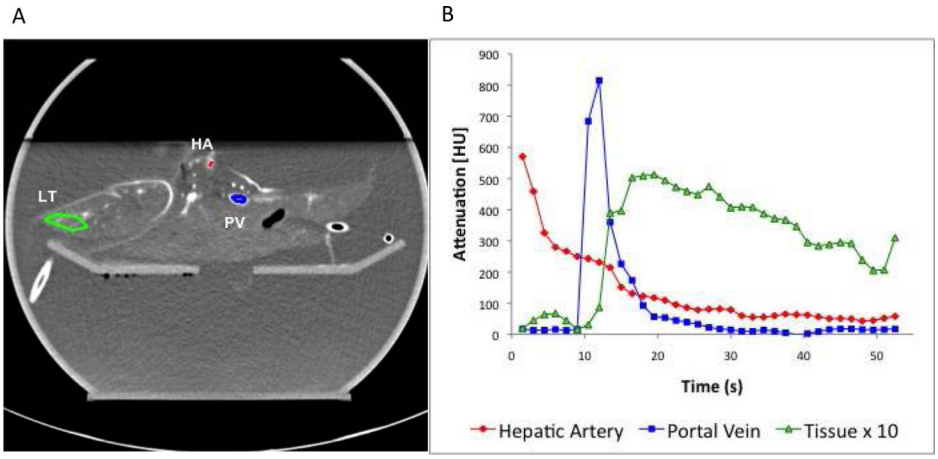

Figure 6. Dual Input Liver Perfusion CT

Representative histology from porcine liver phantom 4 months after initial perfusion and fixation at the completion of imaging experiments. Hepatic architecture and cytologic features are well preserved and intact after contrast-enhanced imaging 60+ times. Branches of the hepatic artery (HA), portal vein (PV) and central vein (CV) are patent with preservation of endothelial cells. H&E slides from the periphery of the left lateral lobe. **(A)** Patent portal tracts and portal triad (10×). **(B)** Patent portal triad (40×) with evidence of contrast material in the portal vein (arrow). **CV** = Central Vein, **HA** = Hepatic Arterial Branch, **PV** = Portal Venous Branch, **BD** = Bile Duct, **PT** = Portal Tracts

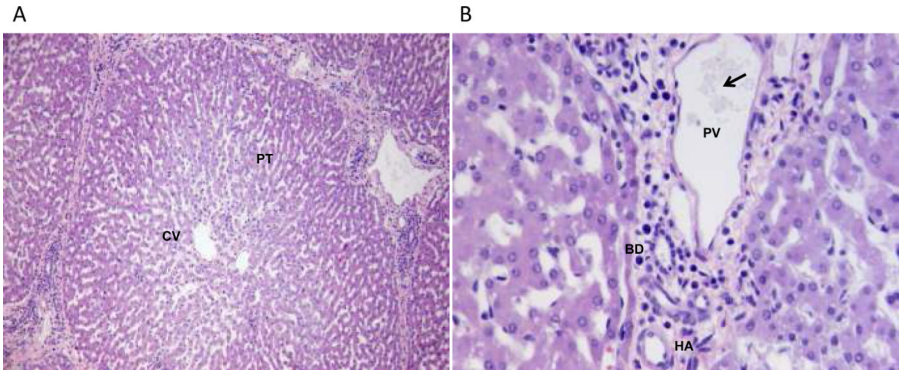

Figure 7. Histology

Simultaneous hepatic arterial and portal venous perfusion. (**A**) Regions of interest (ROIs) segmented onto maximum intensity projection (MIP) over branches of the hepatic artery (red) and portal vein (blue) and liver tissue (green). (**B**) Corresponding time-attenuation-curves (TACs) demonstrate biphasic liver enhancement with the hepatic arterial peak enhancement preceding the portal venous peak enhancement. **Key**: HA= Hepatic Artery (red diamond), PV= Portal Vein (blue square) and LT= Liver Tissue (green triangle).

Table 1

Contrast Injection Protocol for Perfusion CT Protocol A

Input Flow (ml/min)	Contrast Volume (ml)	Injection speed (ml/s)	Injection time (s)
250	3	1	3
375	5	1.5	3.2
500	6	2.0	3
625	8	2.5	3.3
750	9	3.0	3

Table 2

Portal Venous Perfusion Circuit Pressure and Flow

Pressure (mmHg)	Flow (ml/min)
12	200
23	300
33	400
43	500
53	600
62	700
71	800
81	900
93	1000
103	1100
112	1200
123	1300